INVESTIGATION OF THE REACTION OF SOIL TO MOVEMENT BY PLATES AT VARIOUS INCLINED ANGLES BASED ON 2D-DEM
/
基于二维离散元法对倾角条件影响土壤-板接触系统相互作用的研究

Liangyu YUAN， Jun GE *), Chengmao CAO, Kuan QIN, Yan SUN, Liangfei FANG [1]
School of Engineering, Anhui Agricultural University, Hefei, Anhui / China
Tel:(+86) 150 7791 2067; E-mail: gejunahau@ahau.edu.cn
Corresponding author: Ge Jun
DOI: https://doi.org/10.35633/inmateh-73-31

Keywords: *soil-plate interaction system, 2D-DEM, varied inclination angle, Terramechanics*

ABSTRACT
In order to investigate the soil reactions influenced by the single plate with the inclination angles from 0° to 75°, an in-house code of 2D DEM has been developed in this study. An iron flat plate penetrated soil by a constant velocity of 1 mm/s in the study. In the penetration test, the maximum vertical force was 753.8 N which was generated by the 0° plate. In addition, it was found that the less the inclination angle, the greater the vertical force. Furthermore, a greater force in the horizontal direction has been generated at 45° of the inclination angle. This research can provide a theoretical reference for optimizing tools that contact soil, for example, patterns/lugs on wheels, earthmoving blades (such as rotary cultivators, bulldozers, weeding machines etc.) and grouser of tracks.

摘要
本研究旨在利用二维离散元仿真方法对单板倾角从 0°变化到 75°时土壤反力变化进行研究。在仿真试验过程中，钢材料平板以1mm/s 的恒定速度向土壤中贯入。试验结果显示，贯入试验土壤最大反力为 0°板产生的 753.8N，与此同时，还发现垂直反力与板的倾角呈现反比关系，而水平反力峰值出现在倾角 45°左右。这项研究为优化触土工具提供了理论参考，如胎花、推土刀片（旋耕机、推土机、除草机等）和履刺等。

INTRODUCTION
When machines operate under water flow or other weak soil conditions, the running gear needs to produce greater traction, by using lugged wheels, for example *(Holthusen et al., 2018; Md-Tahir et al., 2019; Rasool et al., 2018)*. Meanwhile, those soil conditions, such as the tiller machine in paddy fields, demand machines with a smaller earth contact pressure *(Tian et al., 2021; Jiang et al., 2021)*. Since it is a fundamental problem in the field of terramechanics, research on the influence of lugs or plates on soil reaction forces has always attracted the attention of researchers *(Wong, 2010; Zhu et al., 2023; Ravula et al., 2021)*.

Initially, as described by *Gill & Vanden Berg (1968)* in their book, *Soil Dynamics in Tillage and Traction*, in reaction analysis, the soil was regarded as an isotropic and homogeneous material. The main experimental method for examining the different soil conditions is the soil bin test, and researchers have achieved excellent results when using this method *(Wong, 2001; Wei et al., 2022; Stefanow & Dudziński, 2021)*.

In the Asian region, the water fields have a wide range of soil conditions because of water contents and region differences. Number of studies have been carried out on the interaction between machinery/tools and paddy soil, such as the running gear of rice transplanter/tiller and soil interaction system *(Jia et al., 2016; Nassiraei et al., 2020)*. *Wang et al. (1993, 1995)* conducted two sets of the wider-spaced lugs of the lugged wheel on the cutting resistance of the metal surface in the wheel–soil interaction system. However, they used the fixed lug-wheel, and, therefore, there was no mention of the effect of changes in the inclination angle. *Hermawan et al. (1996, 1997 & 1998)* implemented a series of experiments to investigate the effect of angle changes on single movable lugs, movable lug wheels, and fixed lug wheels under wet loam soil conditions.

[1] *Yuan Liangyu， Stud. Eng.; Ge Jun, Lecturer PhD. Eng.; Cao Chengmao, Prof. PhD. Eng.; Qin Kuan, Assoc. Prof. PhD. Eng.; Sun Yan, Assoc. Prof. M.S. Eng.; Fang Liangfei, Lecturer PhD. Eng.*

However, given the disregard of the effect of lug spacing in those studies, *Watyotha et al. (2001)* investigated the effect of circumferential angle, lug spacing, and wheel slip on forces produced by a cage wheel in a laboratory soil bin, which was filled with a high-moisture-content Bangkok clay soil. They found that changes in the circumferential angle may significantly affect the lateral force, whereas the smallest change or the largest average lug force is generated by the 20° lug spacing. Besides the conventional methods, in consideration of the efficiency and repeatability of the soil test, computer-aided methods have gradually been widely adopted *(Wong, 2001; Zhang et al., 2020)*.

Initially, the FEM was used to investigate the tool/tire-soil interaction system. *Abo-Elnor et al., (2004),* investigated the soil-blade interaction with sandy soil using 3D FEM. The cutting forces were found to be significantly affected by factors such as blade-cutting width, lateral boundary width, and soil swelling. Until present, the FEM is still used to do concerning research on the items as the soil-blade interaction *(Arefi et al., 2022)*. The discrete/distinct element method (DEM) was proposed by *Cundall et al. (1979)*. From then on, it has been used to investigate the tool/tire-soil interaction system, especially the soil under the condition of a low moisture content *(Ucgull & Saunders, 2020)*. Furthermore, some situations that are practically difficult to achieve in reality, such as the continuous movement of soil particles under tires/tools, can be easily investigated by DEM *(Nakanishi et al., 2020; Ravula et al., 2021; Jiang et al., 2017)*. Researchers also utilized the DEM to study the plate/blade-soil interaction system. For example, *Tsuji et al., (2012),* conducted research on the soil-pushing behavior of a bulldozer blade using a 3D DEM simulation. The result indicated that the size of the cohesive bond force significantly affected the behavior of the particles. However, there are few researchers focused on the effects of the plate inclination angle on soil action and force, though some researchers have conducted soil experiments on the impact of the plate/blade inclination angle. *Yang et al., (2014),* carried out an experiment that focused on the change of the plate under different inclination angles and movement directions. Base on the aforementioned and previous research *(Ge et al., 2019)*, the purpose is to investigate the effects of the plate inclination angle, from 0° to 75°, on soil reaction forces using the two-dimensional (2D) DEM approach in this study.

A non-cohesive soil DEM model and a 5 × 77 × 100 mm plate have been used for this study. The simulation consisted of two parts: calibrate and determine the parameters and moduli for soil particles; and the plate penetrating the soil at a certain depth with different inclined plates.

MATERIALS AND METHODS

First, a soil model should be established, as it is the foundation of the DEM simulation. An in-house 2D DEM code has been developed with a plate-soil system. As a 2D DEM was used in this study, the particles were treated as circular rigid bodies. The study aimed to understand the effect of the plate inclination angle, and the soil model was treated as a linear contact model. To calibrate the soil model, a penetration experiment needed to be performed first.

Soil-soil band

Contact detection is a prerequisite for the calculation of interaction forces between elements *(Zang & Zhao, 2013)*. As mentioned in *INTRODUCTION*, non-cohesive soil was used in this study. These soil particles were piled up layer by layer and were aggregated to form a compound test soil *(Horabik & Molenda, 2016)*.

For DEM simulation, the macro-scale forces are determined by the microscopic relationship between particles. In this study, every soil particle was regarded as a rigid solid, and the algorithm could be illustrated by an elastoplastic system consisting of spring and damping, as shown in Fig. 1.

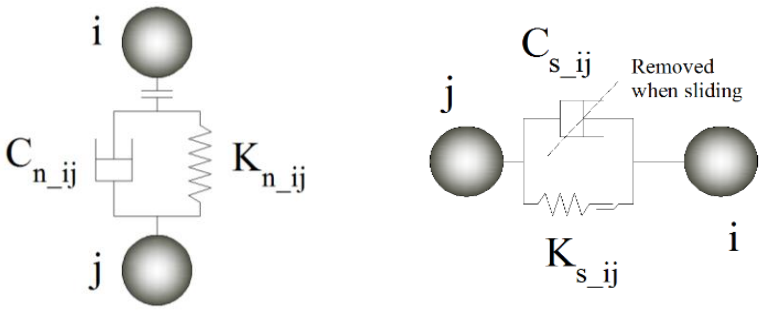

Fig. 1 – Contact model for particles in 2D-DEM
(a) – in normal direction, (b) – in tangential direction

On the basis of the model shown in Fig. 1, it can be seen that the force between particles i and j was divided into two directions: the normal direction and the tangential direction. If the force on particle i in the normal direction is represented by F_{n_i} and the force of the same particle in the tangential direction is represented by F_{s_i}, F_{n_i} and F_{s_i} can be calculated by Equations (1) and (2), as follows:

$$F_{n\_i} = K_{n\_ij}\mu_{n\_ij} + C_{n\_ij}v_{n\_ij} \quad (1)$$

where:

C_{n_ij} and K_{n_ij} are the coefficients of damping and elasticity in the normal direction, respectively. The parameter μ_{n_ij} is the relative displacement of particles i to j in the normal direction, which is illustrated in Fig. 2, and the parameter v_{n_ij} is the relative velocity of particles in the normal direction.

$$F_{s\_i} = \begin{cases} K_{s_{ij}}(\Delta x_{pre} + \Delta x) + C_{s\_ij}v_{s\_ij} & (f_s < \mu f_n) \\ \mu f_n + C_{s\_ij}v_{s\_ij} & (f_s \geq \mu f_n) \end{cases} \quad (2)$$

where:

C_{s_ij} and K_{s_ij} are the coefficients of damping and elasticity in the tangential direction, respectively. Δx_{pre} is the displacement from the previous step, and Δx is the displacement from the previous step to the present step, which is illustrated in Fig. 2. The parameter of $v_{s\text{-}ij}$ is the relative velocity from the previous step to the present step. Equation (2) contains a judgment between f_s and μf_n. μ is the frictional modulus between particles i and j, and the normal force f_n is calculated by Equation (3). f_s is the initial time force, which can be expressed by Equation (4), as follows:

$$f_n = K_{n\_ij}\mu_{n\_ij} \quad (3)$$

$$f_s = f_s^0 + K_{s\_ij}\Delta x \quad (4)$$

where: f_0^s is the force at the previous step.

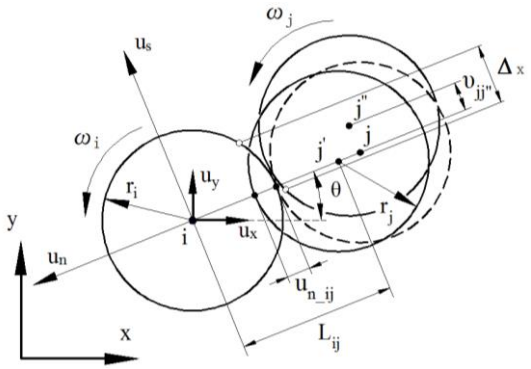

Fig. 2 – The position (displacement) changes in the normal and tangential directions

In Fig. 2, it can be seen that a global coordinate system x-y and a relative coordinate system u_s-u_n have been established to calculate the banding force and moment between particles i and j. In addition, particles i and j have an angular velocity of ω_i and ω_j, respectively. On the basis of these, there should be a rolling resistance moment M_{ij} between the two particles. Specifically, in this study, the parameter M_{ij} was obtained by Equation (5), as follows:

$$M_{ij} = -\alpha b f_n \quad (5)$$

where: f_n is the same parameter as that shown in Equation (3), and α is a constant coefficient of the resistance moment. Parameter b is half the contact length at the overlap between the two particles. If there is an arbitrary element k, the motions of this element should be governed by Newton's second law for the 2D DEM algorithm, as expressed in Equation (6):

$$\begin{cases} m_k \dot{v}_k = F_k \\ I_k \dot{\omega}_k = M_k \end{cases} \quad (6)$$

where:

m_k and I_k are the mass and the inertia moment of element k, respectively. v_k and ω_k are the velocity and the angular velocity of element k, respectively. Parameter F_k represents the resultant force on element k; meanwhile, the resultant moment on element k is represented by M_k.

Soil-plate interaction

The plate had a rectangular shape, which consisted of circular shapes, as shown in Fig. 3.

Soil particles are checked to see whether they were in contact with the plate or not. If contact is detected, the interaction relationship and mechanical algorithm are the same as those introduced in last section. If a total number of *nn* particles were in contact with the plate, the force acting on the plate could be calculated and expressed as follows:

$$\begin{cases} F_x = \sum_0^{nn} F_i^x & (x-axis) \\ F_y = \sum_0^{nn} F_i^y & (y-axis) \end{cases} \quad (7)$$

In Equation (7):

F_x and F_y are the respective force components on the plate in the direction of the x-axis and the y-axis.

F_i^x and F_i^y represent the component force on a single element when in contact with the plate.

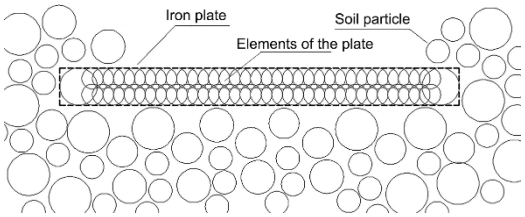

Fig. 3 – Description of the iron plate in the 2D-DEM

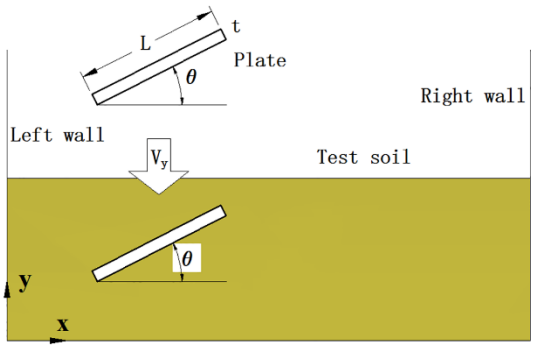

Fig. 4 – Movement of the plate in the soil bin

Experiment and parameter determination

Generally, there are two methods for calibrating the parameters of the DEM soil model: the first method is to repeat the tests on numerous occasions, and after every test, compare the results and check whether they are close to the results of either the in situ measurements or the laboratory experiments; the second method directly determines the input parameters to be equal to the soil test results *(Coetzee, 2019)*. In this study, the first method was utilized.

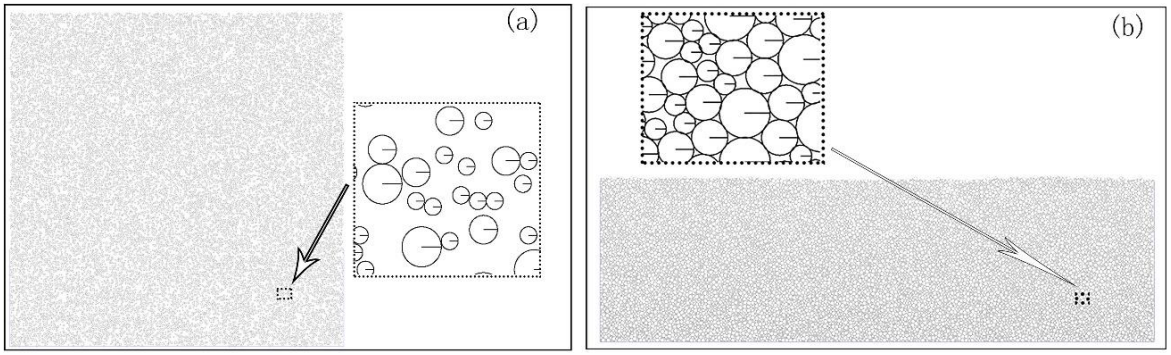

Fig. 5 – Soil particles have been packed in the soil bin:

a) - The soil particles are randomly distributed initially; b) - The particles were settled after a free-falling process

Table 1

Soil parameters in DEM test 4

Items	Value	Unit
Particle number	14,973	
Particle density	2,600	kg/m3
Diameters of particles	1.5; 2.5; 3.5	mm
Frictional modulus	0.48	
Elastic modulus Kn, Ks	50,000, 12,500	N/m

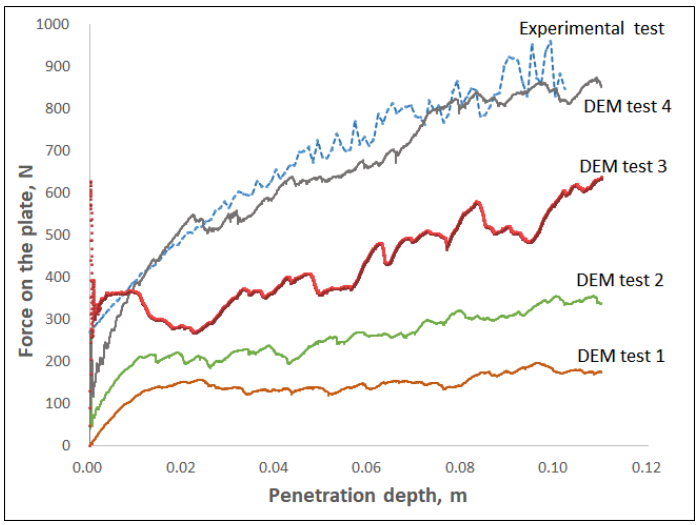

Fig. 6 – A series of DEM trial tests compared with the laboratory experiment

Before conducting the simulation test, a laboratory experiment of penetration testing was performed. The plate, with dimensions of 5 × 77 × 100 mm (thickness × width × length), was set horizontally above the soil surface in the soil bin. The results of the experiment are shown in Fig. 6. In the simulation, according to the established particle–particle bonding rules, a total of 14,973 soil elements were deposited in a soil bin that was 1 m in length, 1 m in height, and 0.3 m in width, as shown in Fig. 5. As a plate with an inclination angle of 0° was used for calibration, the plate was set just above the position of the highest soil particles. After a series of simulation tests, the reaction force results were plotted on a graph, as shown in Fig. 6.

Based on Fig. 6, DEM test 4 matches the laboratory results. The maximum value of the reaction force was 964.87 N in the laboratory experimental test, and it was 873.0 N in DEM test 4. Moreover, the increasing slopes were also similar to each other, DEM test 4 was still considered to be close enough to the laboratory results. Therefore, the soil model with the equivalent parameters of DEM test 4, as shown in Table 1, were used for the planned DEM tests.

RESULTS

A plate with dimensions of 77 × 100 × 5 mm was determined for the DEM tests. After the soil model was calibrated, the plates with 0°, 15°, 30°, 45°, 60° and 75° inclination angles were used for the experiments. The results of the DEM experiments are shown in Fig. 7.

Fig. 7 shows the stress distribution of soil disturbed by plates at different inclination angles during soil penetration at a depth of 100 mm. This demonstrates that the soil reacted to the plate penetration, and when the inclination angle was changed, the soil reacted differently. When the inclination angle changed from 0° to 75°, the forces exerted on the plate were recorded, and the relationship between the forces and the penetration depth is shown in Fig. 8a and Fig. 8b.

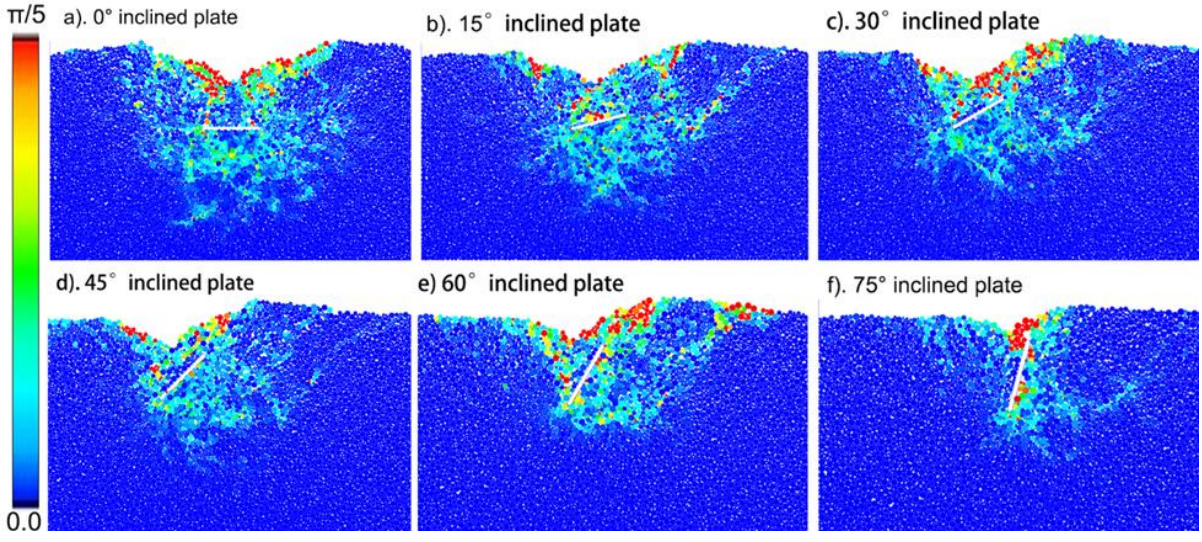

Fig. 7 – Plates with various inclination angles penetrated into the soil at a depth of 100 mm

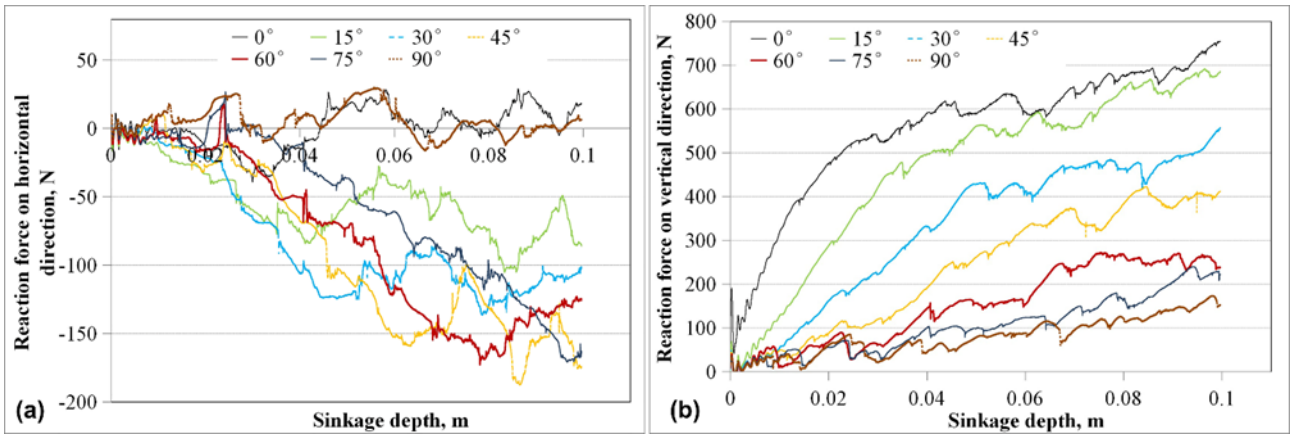

Fig. 8 – Relationship between the forces exerted on the plates and the penetration depth:
(a) - in the horizontal direction, (b) - in the vertical direction

In Fig. 4, it can be seen that the x-axis was in the horizontal direction and the y-axis was in the vertical direction. As shown in Fig. 8a, the horizontal force components of the plates with inclination angles of 0° and 90° have a similar trend with an increasing penetration depth, and their values are close to 0 N. The remaining plates, with inclination angles at 15°, 30°, 45°, 60°, and 75°, are similar to those with angles of 0° and 90° when the penetration depth was < 25 mm. However, if the depth was >25 mm, the horizontal force components at inclination angles of 15° and 30° decreased with an increase in penetration depth, until a depth of approximately 50 mm, and then, they almost kept at 70 and 110 N, respectively, until the plate ceased. In contrast, the plates with inclination angles of 45°, 60°, and 75° decreased almost proportionally to an increase in the penetration depth above 25 mm. The minimum value of the force, −187.6 N, could be achieved using a 45° inclination plate at a depth of 86.6 mm.

Unlike Fig. 8a, Fig. 8b shows that the vertical force components of different inclination plates separated from each other. In addition, the greater the inclination angle, the lower the force value. Except for the 0° plate, under a certain slope rate, the force component of all the plates increased with an increase in penetration depth. In the case of the 0° plate, the force component increased rapidly at a depth of under 25 mm and then increased only gradually with a subsequent increase in depth. The maximum value of the force component was 753.8 N at a depth of 100 mm.

During the penetration process, the relationship between the soil reaction force and the inclination angle has been plotted on a graph, as shown in Fig. 9.

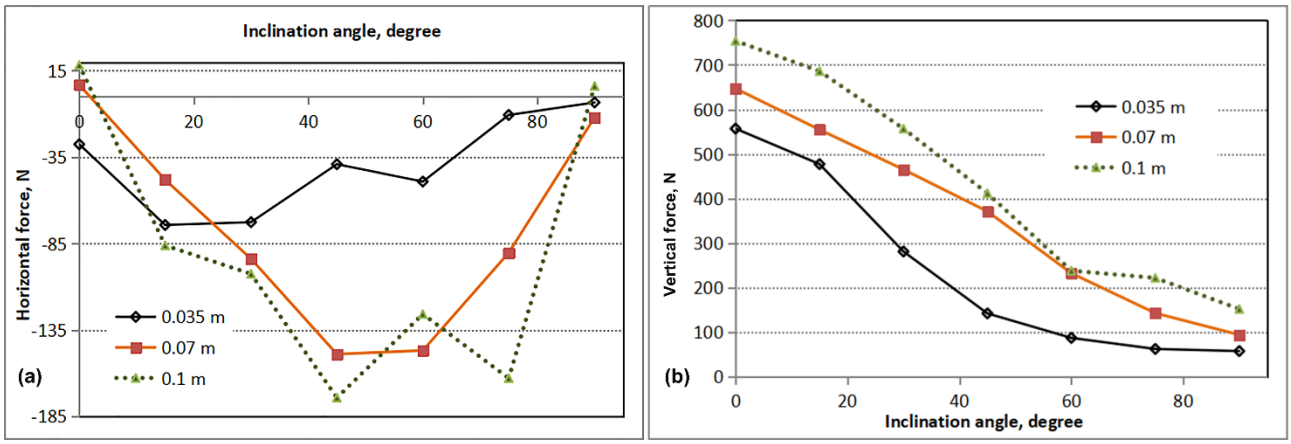

Fig. 9 – The relationship of forces and inclination angle
(a) *- in the horizontal direction, (b) - in the vertical direction*

It can be seen from Fig. 9 that depths of 35, 70, and 100 mm were studied. The figure shows that a change in the inclination angle has a limited effect on the horizontal force component at a depth of 35 mm.

However, if the depths are at 70 or 100 mm, the relationship between the force and the change in depth is similar to a parabolic curve, and the minimum value of the force occurs, in both cases, at an inclination angle of 45°. However, according to Fig. 9b, the vertical force components have a close relationship with changes in the inclination angle. At all depth levels, the perpendicular plate produced the lowest soil reaction force. It can also be seen that a plate with an inclination angle that is perpendicular to the soil surface produces a lower resistance force, as shown in Figs 8 and 9.

CONCLUSIONS

In this study, a non-cohesive DEM soil model was used, calibrated by laboratory penetration experiments. Using this soil model and a plate with dimensions of 5 × 77 × 100 mm, the effects of changes to the inclination angle on the forces generated during a penetration test were investigated. Based on the results of the DEM simulation and the discussion introduced in section 3, the following concluding remarks can be made:

(1) The 2D DEM method is sufficient to meet the research needs for investigating the soil reaction forces, which are affected by changing inclination angles. The whole process has been successfully carried out in this study.

(2) During the penetration process, the maximum value of the vertical force component was 753.8 N, which was generated by a 0° inclination angle plate at a depth of 100 mm, at which point the penetration test was stopped. It was found that the greater the inclination angle, the greater the vertical force.

(3) For the movement of a bulldozer blade, the vertical angle should be maintained to minimize resistance. If the lugs on the tire/track are considered, the inclination angle should be closer to 45° to generate a greater traction force.

ACKNOWLEDGEMENT

This research was supported by the project of the Natural Science Foundation of Anhui Province (2308085ME160).

REFERENCES

[1] Abo-Elnor, M., Hamilton, R., Boyle, J. T. (2004). Simulation of soil–blade interaction for sandy soil using advanced 3D finite element analysis, *Soil and Tillage Research*, Vol. 75, Iss. 1, pp. 61-73. Egypt;

[2] Arefi, M., Karparvarfard, S. H., Azimi-Nejadian, H., Naderi-Boldaji, M. (2022). Draught force prediction from soil relative density and relative water content for a non-winged chisel blade using finite element modelling, *Journal of Terramechanics*, Vol. 100, pp. 73-80. Iran;

[3] Coetzee, C. J. (2019). Particle upscaling: Calibration and validation of the discrete element method, *Powder Technology,* Vol. 344, pp. 487-503. South Africa;

[4] Cundall, P. A., Strack, O. D. L. (1979). A discrete numerical model for granular assemblies, *Geotechnique*, Vol. 29, Iss. 1, pp. 47-65. UK;

[5] Ge, J., Zhang, D. S., Wang, X. L., Cao, C. M., Fang, L. F., Duan, Y. M. (2019). Tractive performances of single grouser shoe affected by different soils with varied moisture contents, *Advances in Mechanical Engineering*, Vol. 11, Iss. 5, no.1687814019849133. Hefei/China;

[6] Gill, W. R., Berg, G. E. V. (1968). Soil dynamics in tillage and traction, Agricultural Research Service, U.S. Department of Agriculture. *America Agriculture Handbook No. 316*. United States;

[7] Hermawan, W., Oida, A., Yamazaki, M. (1996). Measurement of soil reaction forces on a single movable lug, Journal of Terramechanics, Vol. 33, Iss. 2, pp. 91-101. Japan;

[8] Hermawan, W., Oida, A., Yamazaki, M. (1997). The characteristics of soil reaction forces on a single movable lug, *Journal of Terramechanics*, Vol. 34, Iss. 1, pp. 23-35. Japan;

[9] Hermawan, W., Yamazaki, M., Oida, A. (1998). Experimental analysis of soil reaction on a lug of a movable lug wheel, *Journal of Terramechanics*, Vol. 35, Iss. 2, pp. 119-135. Indonesia;

[10] Holthusen, D., Brandt, A. A., Reichert, J. M., Horn, R., Fleige, H., Zink. A. (2018). Soil functions and in situ stress distribution in subtropical soils as affected by land use, vehicle type, tire inflation pressure and plant residue removal, *Soil and Tillage Research,* Vol. 184, pp. 78-92. Brazil;

[11] Horabik, J., Molenda, M. (2016). Parameters and contact models for DEM simulations of agricultural granular materials: A review, *Biosystems Engineering*, Vol. 147, pp. 206-225. Poland;

[12] Jia, H., Guo, M., Yu, H., Li, Y., Feng, X., Zhao, J., Qi, J. (2016). An adaptable tillage depth monitoring system for tillage machine, *Biosystems Engineering*, Vol. 151, pp. 187-199. Jilin/China;
[13] Jiang, M., He, J., Wang, J., Zhou, Y., Zhu, F. (2017). Discrete element analysis of the mechanical properties of deep-sea methane hydrate-bearing soils considering interparticle bond thickness, *Comptes Rendus Mécanique,* Vol. 345, pp. 868-889. Shanghai/China;
[14] Jiang, Q. J., He, Z. L., Wang, Y. W., Wang. J. (2021). Optimizing the working performance of a boat-type tractor using central composite rotatable design and response surface method, *Computers and Electronics in Agriculture*, Vol. 181, 105944. Hangzhou/China;
[15] Md-Tahir, H., Zhang, J., Xia, J., Zhang, C., Zhou, H., Zhu, Y. (2019). Rigid lugged wheel for conventional agricultural wheeled tractors - Optimising traction performance and wheel–soil interaction in field operations, *Biosystems Engineering,* Vol. 188, pp.14-23. Wuhan/China;
[16] Nakanishi, R., Nakashima, H., Miyasaka, J., Ohdoi, K. (2020). Tractive performance analysis of a lugged wheel by open-source 3D DEM software, *Journal of Terramechanics,* Vol. 92, pp. 51-65. Japan;
[17] Nassiraei, A. A. F., Skonieczny, K. (2020). Grousers improve drawbar pull by reducing resistance and generating thrust at the front of a wheel, *Journal of Terramechanics*, Vol. 91, pp. 73-84. Canada;
[18] Rasool, S., Raheman, H. (2018). Improving the tractive performance of walking tractors using rubber tracks, *Biosystems Engineering,* Vol. 167, pp. 51-62. India;
[19] Ravula, P., Acar, G., Balachandran, B. (2021). Discrete element method-based studies on dynamic interactions of a lugged wheel with granular media, *Journal of Terramechanics*, Vol. 94, pp. 49-62. United States;
[20] Stefanow, D., Dudziński, P. A. (2021). Soil shear strength determination methods – State of the art, *Soil and Tillage Research*, Vol. 208, 104881. Poland;
[21] Tsuji, T., Nakagawa, Y., Matsumoto, N., Kadono, Y., Takayama, T., Tanaka, T. (2012). 3-D DEM simulation of cohesive soil-pushing behavior by bulldozer blade, *Journal of Terramechanics,* Vol. 49, Iss. 1, pp. 37-47. Japan;
[22] Ucgul, M., Saunders, C. (2020). Simulation of tillage forces and furrow profile during soil-mouldboard plough interaction using discrete element modelling, *Biosystems Engineering,* Vol. 190, pp. 58-70. Australia;
[23] Wang, X. L., Yamazaki, M., Tanaka, T. (1993). Dynamic behaviour of an open lugged wheel under paddy soil conditions, *Journal of Terramechanics*, Vol. 30, Iss. 3, pp. 191-203. Japan;
[24] Wang, X. L., Yamazaki, M., Tanaka, T. (1995). Characteristics of soil reactions of an open lugged wheel under paddy soil conditions, *Journal of Terramechanics,* Vol. 32, Iss. 3, pp. 115-125. Japan;
[25] Watyotha, C., Gee-Clough, D., Salokhe, V. M. (2001). Effect of circumferential angle, lug spacing and slip on lug wheel forces, *Journal of Terramechanics*, Vol. 38, Iss. 1, pp. 1-14. Thailand;
[26] Wei, H. Q., Ai, Q., Zhao, W. Q., Zhang, Y. T. (2022). Modelling and experimental validation of an EV torque distribution strategy towards active safety and energy efficiency*, Energy,* Vol. 239, Part A, 121953. Beijing/China;
[27] Wong, J. Y. (2001). Theory of ground vehicles. 3rd ed. New York: *John Wiley & Sons*. Canada;
[28] Wong, J. Y. (2010). Terramechanics and off road vehicle engineering: Terrain behavior, off-road vehicle performance and design. 2nd ed. *UK: Elsevier*. Canada;
[29] Yang, Y., Sun, Y., Ma, S., Yamamoto, R. (2014). Characteristics of normal and tangential forces acting on a single lug during translational motion in sandy soil, *Journal of Terramechanics,* Vol. 55, pp. 47-59. Japan;
[30] Zang, M., Zhao, C. (2013). Numerical Simulation of Rigid Wheel Running Behavior on Sand Terrain on sand terrain, Singapore, *APCOM & ISCM*. Guangzhou/China;
[31] Zhang, R., Pang, H., Dong, W. C., Li, T., Liu, F., Zhang, H., Hu, Z. Y., Li, J. Q. (2020). Three-dimensional Discrete Element Method simulation system of the interaction between irregular structure wheel and lunar soil simulant, *Advances in Engineering Software*, Vol. 148, 102873. Shanghai/China;
[32] Zhu, J., Shen, Y., Hao, P., Liu, J., Li, Y., Wang, K., Zou, M. (2023). Modeling of flexible metal wheel for pressurized lunar rover and traction performance prediction. *Journal of Field Robotics*, Vol. 40, Issue 8, pp. 2030-2041. Tianjin/China